

A robust statistics-based global energy function for the alignment of serially acquired autoradiographic sections

Christophoros Nikou^{a,c}, Fabrice Heitz^{c,*}, Astrid Nehlig^b, Izzie Jacques Namer^a,
Jean-Paul Armspach^a

^a *Université Louis Pasteur (Strasbourg I), Institut de Physique Biologique, Faculté de Médecine, ULP-CNRS UMR 7004, 4 rue Kirschleger, 67085 Strasbourg CEDEX, France*

^b *INSERM U398, Faculté de Médecine, 11, rue Humann, 67085 Strasbourg CEDEX, France*

^c *Université Louis Pasteur (Strasbourg I), Laboratoire des Sciences de l'Image, de l'Informatique et de la Télédétection, ULP-CNRS UMR 7005, 4. Bd. Sébastien Brant, 67400 Illkirch, France*

Received 27 August 2002; received in revised form 13 December 2002; accepted 16 December 2002

Abstract

Autoradiographic analysis of the functional changes occurring in the rat brain are most often performed on coronal sections that allow a good insight into the events occurring at the structural level but lacks the 3D context which is necessary to fully understand the involvement of the brain structures in specific situations like focal seizures with or without generalization. Therefore a robust, fully-automated algorithm for the registration of serially acquired autoradiographic sections is presented. The method accounts for the main difficulties of autoradiographic alignment: corrupted data (cuts and tears), dissimilarities or discontinuities between slices, non parallel or missing slices. The approach relies on the minimization of a global energy function based on robust statistics. The energy function measures the similarity between a slice and its neighborhood in the 3D volume. No particular direction is privileged in the method, so that global offsets, biases in the estimation or error propagations are avoided. The method is evaluated qualitatively and quantitatively on real autoradiographic data. Rat brain autoradiographic volumes are reconstructed with registration errors less than 1 degree in rotation and less than 1 pixel in translation.

© 2003 Elsevier Science B.V. All rights reserved.

Keywords: Serially acquired images; Alignment; Image registration; Pixel similarity measure; Robust estimation; Three dimensional reconstruction; Autoradiography

1. Introduction

Three-dimensional reconstruction of brain structures is now an integral part of neuroscience research. In autoradiography, samples of brain tissue are generated by sectioning and image data are acquired in 2D format. Reconstitution of such data sets into 3D volumes, via the registrations of 2D sections, has gained an increasing interest for the mapping of image data to anatomical references. Indeed, cerebral functional changes occurring in most situations involve only a limited number of brain structures. The usual 2D analysis of metabolic or

circulatory changes on only one section (e.g. coronal section) allows to identify the structures of interest but does not give an easy insight into the network that is involved in a particular situation, mainly when the changes occur only in a limited number of structures and spread from forebrain to brainstem. The 3D reconstruction will for example be very useful to identify the networks involved in epileptic seizures, especially when seizures are only focal or propagate to a limited number of regions outside of the focus.

Several registration algorithms have been proposed to register serially acquired slices. A review of medical image registration methods is presented in Gottesfeld-Brown (1992), Maintz and Viergever (1998) and Van den Elsen et al. (1993). A review of 3D reconstruction from autoradiographs, as well as a comparison between standard methods may be found in Hess et al. (1998).

* Corresponding author. Tel.: +33-3-9024-4487; fax: +33-3-9024-4342.

E-mail address: heitz@lsiit.u-strasbg.fr (F. Heitz).

The principal autoradiography alignment methods may be classified in the following categories: (a) fiducial marker or artificial landmark-based methods (Goldszal et al., 1995; Hess et al., 1998; Toga and Arnica, 1985); (b) principal axes alignment (Hess et al., 1998; Hibbard and Hawkins, 1988); (c) feature-based methods, using contours, crest lines or characteristic points extracted from the images (Hibbard and Hawkins, 1988; Rangarajan et al., 1997; Zhao et al., 1993); (d) grey level-based registration techniques using the intensities of the whole image, through similarity or correlation functions (Andreasen et al., 1992; Hess et al., 1998; Kim et al., 1997; Ourselin et al., 1998; Zhao et al., 1993). The above mentioned techniques do not simultaneously consider the two major difficulties involved in autoradiographic data registration.

At first, consecutive slices may differ significantly due to distortions, cuts, tears and orientation differences (slices may be non-parallel) (see Fig. 2 for a typical example). Consecutive slices are also naturally dissimilar, even if the data have not been corrupted, since 2D sections of possibly discontinuous 3D anatomical structures are imaged. Dissimilarities are more pronounced when distant slices are involved in the registration. From this point of view, a registration method must be robust to missing data and outlying measurements (Ourselin et al., 1998; Zhao et al., 1993).

Besides, registering the slices sequentially (the second with respect to the first, the third with respect to the second, etc.) leads to different types of misregistrations. If an error occurs in the registration of a slice with respect to the preceding slice, this error will propagate through the whole volume. As a consequence, if the number of slices to be registered is large, a global offset of the volume may be observed, due to error accumulation (Andreasen et al., 1992; Hess et al., 1998).

The approach proposed in this paper addresses the above mentioned shortcomings. A global energy function, having as variables the 2D rigid transformation parameters of all the 2D slices in the 3D volume, is optimized. The energy function is isotropic. As a consequence, no direction is privileged in the registration process and the final alignment is not biased. Global energy functions are a powerful tool in computer vision applications (Heitz et al., 1994) but, to our knowledge, they have not yet been considered for the registration of serially acquired slices. Besides, the global energy function considered here is associated with a robust pixel similarity metric (Nikou et al., 1998) rejecting outlying measures. By these means, non-overlapping and corrupted slices are correctly registered.

The remainder of the paper is organized as follows. The global energy function formulation and the associated registration algorithm is presented in Section 2. The robust pixel similarity measure is described in

Section 3. Experimental results are presented in Section 4 and conclusions are drawn in Section 5.

2. A global energy function formulation

Before presenting the registration method, we introduce the notations used in our formulation. A set of 2D serially acquired slices is represented by

$$V = \{I_i | i = 1, \dots, N\} \quad (1)$$

where I_i is a slice (a 2D image) and N denotes the total number of slices. A pixel of a 2D slice is represented by $p = (x, y)$ so that $I_i(p)$ corresponds to the grey level of pixel p of slice I_i . n_x and n_y designate the number of pixels of each slice in the horizontal and vertical direction respectively.

We consider two-dimensional rigid registration, which consists in estimating the rigid transformation parameters (translations t_x , t_y and rotation through an angle θ) that have to be applied to the image to be registered (floating image) so that it matches a reference image. Let us notice that non-parallelism induces a shear transformation between slices. A proper way to handle this problem would consist in taking into account this distortion by adopting a higher order (for instance an affine) transformation model. This has not been considered here, essentially to keep the computational cost to an acceptable level. As will be seen in the following, the robust estimator is able to cope with dissimilarities induced by the non-parallelism and that are not taken into account by the alignment model.

In the approach proposed here, the registration of the 2D sections, within the 3D volume, is considered globally by minimizing an energy function, which expresses the similarity between two arbitrary sections. The 2D sections are considered pair-wise, using the following definition for the global similarity measure:

$$E(\Theta) = \sum_{i=1}^N \sum_{j=1}^N \sum_{p=1}^{n_x \times n_y} f(I_i(T_{\Theta_i}(p)), I_j(T_{\Theta_j}(p))) \quad (2)$$

where $f(\cdot, \cdot)$ is a similarity metric, I_k denotes slice k and T_{Θ_k} designates a rigid transformation with parameters $\Theta_k = \{t_x^k, t_y^k, \theta^k\}$. The parameter vector to be estimated is denoted $\Theta = \{\Theta_1, \Theta_2, \dots, \Theta_N\}$.

It is common sense that distant slices present little similarity, due to anatomy. Therefore, we have limited the support region of function $f(\cdot, \cdot)$ to a region of radius $R > 0$ centered at each slice and set:

$$f(I_i(T_{\Theta_i}(p)), I_j(T_{\Theta_j}(p))) = 0, \quad \text{for } |i - j| > R \text{ or } i = j \quad (3)$$

Besides, we have adopted symmetric similarity functions $f(\cdot, \cdot)$, in order to preserve isotropy in the registration process:

$$\begin{aligned}
& f(I_i(T_{\Theta_i}(p)), I_j(T_{\Theta_j}(p))) \\
& = f(I_j(T_{\Theta_j}(p)), I_i(T_{\Theta_i}(p))) \quad \text{with:} \\
& f(I_i(T_{\Theta_i}(p)), I_i(T_{\Theta_i}(p))) = 0
\end{aligned} \tag{4}$$

The global minimization problem thus reduces to:

$$\begin{aligned}
\hat{\Theta} & = \arg \min_{\Theta} E(\Theta) \\
& = \arg \min_{\Theta} \sum_{i=1}^{N-1} \sum_{i < j \leq \min(i+R, N)} \\
& \quad \times \sum_{p=1}^{n_x \times n_y} f(I_i(T_{\Theta_i}(p)), I_j(T_{\Theta_j}(p)))
\end{aligned} \tag{5}$$

Without additional constraints, the optimization problem (5) has clearly an infinite number of solutions (if the set of rigid transformations $\{T_{\hat{\Theta}_1}, T_{\hat{\Theta}_2}, \dots, T_{\hat{\Theta}_N}\}$ is a solution, the same holds true for $\{T_{\hat{\Theta}_1} \circ T_{\Delta}, T_{\hat{\Theta}_2} \circ T_{\Delta}, \dots, T_{\hat{\Theta}_N} \circ T_{\Delta}\}$, where T_{Δ} is an arbitrary 2D rigid transformation). To remove this ambiguity, the transformation $T_{\hat{\Theta}_k}$ applied to an arbitrary chosen slice k is constrained to the identity transformation (we have chosen $k = N/2$ in our implementation). As a result, there are $3(N-1)$ parameters to estimate.

The algorithm used to minimize the objective function (5) may be described as following:

- **do** until convergence.
 - declare all slices unvisited.
 - **do** until all slices are declared visited.
 - randomly choose an unvisited slice $I_i \in V$.
 - update the rigid transformation parameters T_{Θ_i} bringing into alignment slice I_i with the other slices in the neighborhood of i , by minimization of the following local energy function:

$$\begin{aligned}
E_i(\Theta_i) & \stackrel{\text{def}}{=} \sum_{\substack{\max(1, i-R) \leq j \leq \min(i+R, N) \\ j \neq i}} \\
& \quad \times \sum_{p=1}^{n_x \times n_y} f(I_i(T_{\Theta_i}(p)), I_j(T_{\Theta_j}(p)))
\end{aligned} \tag{6}$$

- declare slice I_i visited.
- **end do**
- **end do**

In our current implementation, the minimization of the local energy function (6) has been conducted by the standard variable-size sequential simplex optimization due to Nelder and Mead (Walters et al., 1991). This algorithm has the advantage to require only function evaluation, not derivatives and thus may be quickly adapted to a large class of similarity functions. We have adopted the standard implementation described in Press et al. (1992). The drawback of the simplex algorithm is its computational cost: it is planned to replace it by a

more efficient gradient descent or quasi-Newton method. The local energy function (6) for slice i is first minimized with respect to t_x and t_y , then with respect to θ , and the procedure is repeated until convergence. The algorithm is stopped after a specified number of scans on all slices (in practice 15 scans on the complete data set yield a satisfactory compensation of the misregistration).

The optimization method converges towards a local minimum of the local energy function (6) and is guaranteed to decrease the global energy function (5) at each step. It is thus easy to see that the described algorithm converges towards a local minimum (or towards a saddle point) of the initial energy function (2). This local minimum corresponds to a satisfactory registration if the initial alignment of the 2D sections is close enough to the desired solution (if this is not the case, a good initialization may be obtained by a standard coarse alignment technique such as principal axes registration). It is thus not necessary to resort here to greedy global optimization procedures, such as simulated annealing or genetic algorithms (Nikou et al., 1998).

If the algorithm is to be used on a routine basis, the similarity metrics must be forgiving about missing data and outlying measurements, which commonly corrupt autoradiographic data (see Fig. 2). A robust estimator-based similarity metric has been adopted to this end. This robust similarity measure is described in the next section.

3. A robust pixel similarity measure

A standard similarity measure in single modal image registration is based on the quadratic error function:

$$f(I_i(p), I_j(p)) = [I_i(p) - I_j(p)]^2 \tag{7}$$

The quadratic error function, which is closely related to the standard cross-correlation measure, works at best under additive Gaussian noise assumptions. Its limits are now well known (Arun et al., 1987; Umeyama, 1991). It is commonly accepted that least squares or cross-correlation are sensitive to gross differences in images due to incomplete images, missing data, non Gaussian noise or ‘outliers’. Outliers generally contribute too much to the overall solution since outlying points are assigned a high weight by the quadratic error function. When a significant amount of outlying measurements or missing data are present in the images to be registered, inaccurate registrations or even misregistrations are observed. To increase robustness, the cost function must thus be forgiving about outlying measurements.

Robust estimators have become popular in computer vision applications because they have proven effective in tolerating gross outliers in the data (Meer et al., 1990; Stewart, 1997). A review on robust estimators in computer vision may be found in Meer et al. (1990) and Black and Rangarajan (1996).

A standard performance measure for a robust estimator is its breakdown point. The breakdown point is the largest fraction of data that can be arbitrarily bad and will not cause the solution to be arbitrarily bad. The least median of squares regression (Rousseeuw, 1984) relies on the minimization of the median of the squared residuals. The resulting estimator can resist to the effect of nearly 50% of contamination in the data. In the special case of simple regression, it corresponds to finding the narrowest strip covering half of the observations. The MINPRAN algorithm (Stewart, 1997) has also a breakdown point of 50% and relies on random data sampling. These estimators have high breakdown points but also yield a high computational load, since they are based on random data sampling and sorting. Another class of estimators, the M-estimators (Huber, 1981), that have attractive properties (i.e. satisfactory breakdown points and moderate computational cost), have been used in computer vision (Black and Rangarajan, 1996; Odobez and Bouthemy, 1995) and medical imaging (Alexander and Somorjai, 1996; Nikou et al., 1998). This class of robust estimators reduces the optimization problem to a simple, low cost, weighted least squares problem (Black and Rangarajan, 1996; Meer et al., 1990). They have a theoretical breakdown point of $1/(p+1)$, where p is the number of parameters to fit (Meer et al., 1990). In practice, it has been observed, in low dimensional estimation problems (Black and Jepson, 1996; Nikou et al., 1999), that this family of robust estimators can tolerate roughly up to 35–45% of the data as outliers. Thus, M-estimators provide a good compromise between computational complexity and outlier rejection capacity.

In our case, we have used the Geman-McClure robust M-estimator that has successfully been used in Nikou et al. (1998) to match 3D multimodal images of the human brain. The similarity function associated to this estimator is defined by:

$$f(I_i(p), I_j(p), \sigma) \stackrel{\text{def}}{=} \rho(I_i(p) - I_j(p), \sigma) \stackrel{\text{def}}{=} \frac{[I_i(p) - I_j(p)]^2}{[I_i(p) - I_j(p)]^2 + \sigma^2} \quad (8)$$

where σ is a scaling parameter.

The Geman-McClure ρ function (Fig. 1a) has a shape that rejects large residual errors, i.e. it is more forgiving about large residuals than the standard quadratic error function. The influence function (Fig. 1b) is the derivative of function $\rho(\cdot)$ and characterizes the influence of the residuals. As can be seen on Fig. 1(b), as the magnitude

of the residuals increases and grows beyond a point, its influence on the solution begins to decrease and the value of $\rho(\cdot)$ approaches a constant. The scaling parameter σ affects the point at which the influence of outliers begins to decrease. For the error function ρ used here, points p for which:

$$|I_i(T_{\Theta_i}(p)) - I_j(T_{\Theta_j}(p))| \geq \frac{\sigma}{\sqrt{3}}$$

can be viewed as outliers, as the outliers rejection begins where

$$\frac{\partial^2 \rho}{\partial x^2} = 0.$$

The calculation of the rigid transforms parameter vector Θ now involves the minimization of the non-linear cost function:

$$E(\Theta) = \sum_{i=1}^{N-1} \sum_{i < j \leq \min(i+R, N)} \times \sum_{p=1}^{n_x \times n_y} f(I_i(T_{\Theta_i}(p)), I_j(T_{\Theta_j}(p)), \sigma) \quad (9)$$

depending on the scale parameter σ .

A standard strategy (Stewart, 1997; Nikou et al., 1998) consists in starting the optimization procedure with a high value for σ . The value of σ decreases during the minimization process following the formula $\sigma = \alpha \cdot \sigma$ with $0.8 < \alpha < 1$ until σ reaches a predefined value. The effect of this procedure is that initially no data are rejected as outliers and a first, crude solution is obtained. During the following optimization steps the influence of the outliers is gradually reduced by decreasing σ , leading to a reliable estimation of the rigid transformation parameters, which is robust to gross image differences. Another approach, proposed in Odobez and Bouthemy (1995), estimates σ as the variance of the current smallest residual error. At each iteration step, if slice I_m has been selected for the local minimization of (9), σ is computed as follows. At first the slice I_j providing the smallest registration error with slice I_m is found. Then σ is defined as the standard deviation of that residual error:

$$\sigma_m = \min_j \sqrt{\frac{1}{n_x \times n_y} \sum_{p=1}^{n_x \times n_y} [I_m(T_{\Theta_m}(p)) - I_j(T_{\Theta_j}(p))]^2 - \mu_j^2} \quad (10)$$

where:

$$\mu_j = \frac{1}{n_x \times n_y} \sum_{p=1}^{n_x \times n_y} [I_m(T_{\Theta_m}(p)) - I_j(T_{\Theta_j}(p))] \quad (11)$$

and the local energy function, to be minimized becomes:

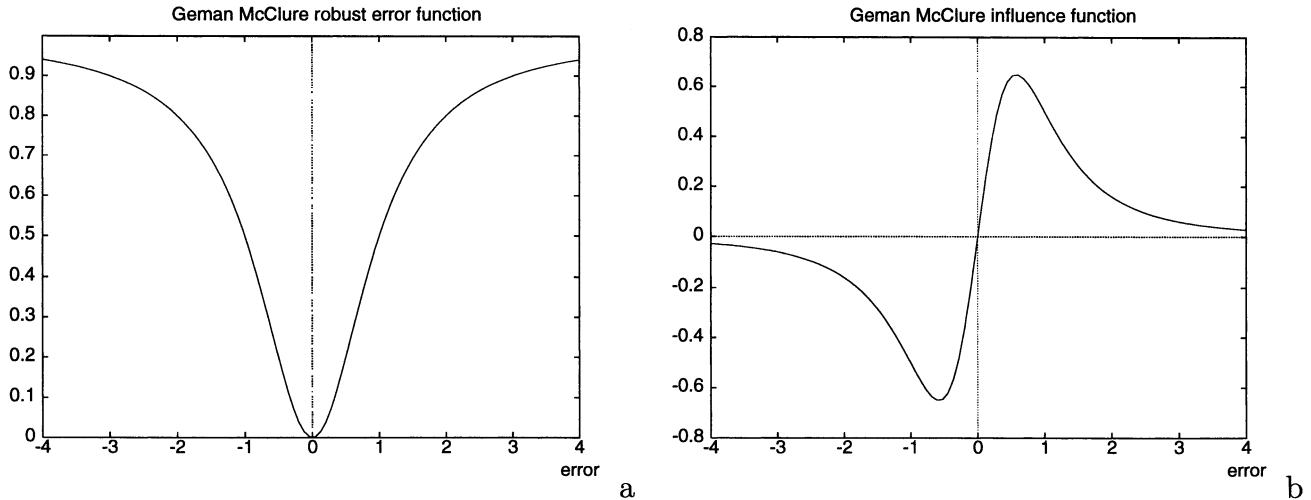


Fig. 1. The Geman-McClure robust similarity function $p(\cdot)$ (a) and its derivative $p'(\cdot)$ (the influence function) (b).

$$E_m(\Theta_m) \stackrel{\text{def}}{=} \sum_{\substack{\max(1, m-R) \leq k \leq \min(m+R, N) \\ k \neq m}} \times \sum_{p=1}^{n_x \times n_y} f(I_m(T_{\Theta_m}(p)), I_k(T_{\Theta_k}(p)), \sigma_m) \quad (12)$$

This second strategy thus automatically decreases the scale parameter σ while the registration is in progress. It gives good results in practice and has been adopted in our implementation.

Finally, a large number of interpolations are involved in the registration process. The accuracy of the rotation and translation parameter estimates is directly related to the accuracy of the underlying interpolation model. Simple approaches such as the nearest neighbor interpolation are commonly used because they are fast and simple to implement, though they produce images with noticeable artifacts. Besides, in our application, as the translation and rotation parameters to compensate have subvoxel values, this type of interpolation is not appropriate. More satisfactory results can be obtained by small-kernel cubic convolution techniques, bilinear, convolution-based interpolation or B-spline-based generalized interpolation (Thevenaz et al., 2000). According to the sampling theory, optimal results are obtained using sinus cardinal interpolation, but at the expense of a high computational cost. As a compromise, we have used a bilinear interpolation technique in the optimization steps. At the end of the algorithm, the registration parameters are refined using a truncated sinus cardinal interpolation. This final interpolation step gives high quality image reconstructions, significantly better than those obtained with the bilinear interpolation.

4. Experimental results

Computation and display were performed on a Hewlett-Packard HP9000/200 workstation by using a 2D–3D image analysis software (MEDIMAX) developed at IPB. This software, running under Unix, is developed in C language and uses the standard graphics interface X11/R6. All registration techniques presented in this paper were implemented under this software environment and are easily available to users.

To evaluate our method, we have first applied the algorithm to the reconstruction of an artificially misaligned human brain acquired by 3D MRI (for which ground truth is readily available). The slices of the original $128 \times 128 \times 128$ MRI volume (pixel size $2 \text{ mm} \times 2 \text{ mm}$, slice thickness 2 mm) were transformed using translations varying from -10 to $+10$ pixels and rotations varying from -10 to $+10$ degrees. The transformations for each slice were random, following a uniform distribution in order not to privilege any slice. The resulting consecutive 2D sections are locally dissimilar, due to discontinuities in the 3D anatomical structures of the brain. Quadratic similarity functions are not able to recover the transformation parameters with subvoxel accuracy in this case. Table 1 presents statistics on the registration errors, obtained with the robust error function. The algorithm revealed robust in registering the locally dissimilar 2D sections, with subvoxel accuracy.

We have also evaluated our method in the alignment of autoradiographic rat brain images presenting dissimilarities due to discontinuities, cuts and tears (Fig. 2). To obtain the initial data set, four contiguous autoradiographic slices were retained, every ten slices. The other slices were not considered, yielding large discontinuities

Table 1

A set of 128 slices of a 3D MRI of a human brain volume were artificially transformed using different rigid transformation parameters

Registration error statistics			
	Δt_x	Δt_y	$\Delta \theta$
Median	0.11	0.12	0.22
Maximum	0.59	0.48	1.25
Mean \pm S.D.	0.24 \pm 0.11	0.18 \pm 0.12	0.40 \pm 0.23

Each slice was randomly transformed using translations varying from -10 to $+10$ pixels and rotations varying from -10 to $+10$ degrees. Different statistics on the errors for the rigid transformation parameters are presented. Translation errors are expressed in pixels and rotation errors in degrees.

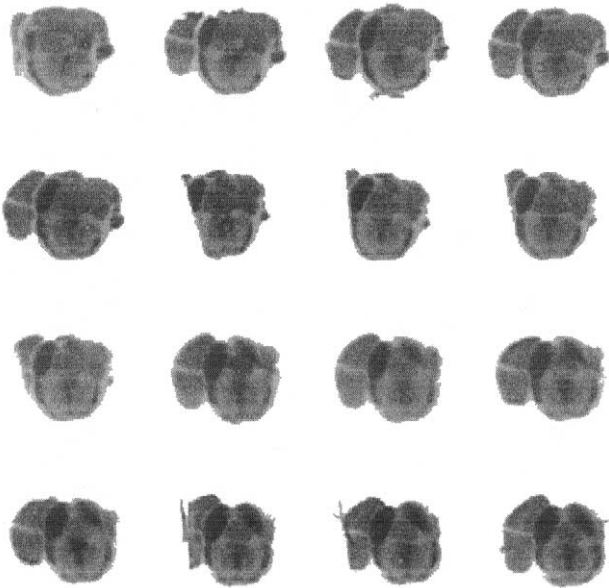


Fig. 2. Consecutive slices of a rat brain autoradiography considered in our experiments. Four autoradiographic images every ten slices are acquired from the same rat introducing discontinuities in the autoradiographic volume. Cuts and tears are also visible on the sequence of slices.

in the data set. An average of 400–600 slices was thus obtained, for each rat volume. These slices were then exposed on films. Each film was scanned and the data files transferred to the HP Unix workstation to be processed. An automated algorithm based on thresholding and labelling extracts from each scanned film the slices. Each slice of the volume has dimensions of 128×128 pixels. The pixel dimensions are $127 \mu \times 127 \mu$ and slice thickness is 20μ . Since large discontinuities are present every four slices, standard registration methods are unable to register the data. Moreover, in general the location of the discontinuities is not known and the number of slices between two discontinuities may also vary accidentally.

At first, a semi-manually registered rat brain volume was created, to provide some ‘ground truth’. The semi-manually registration consisted of three steps:

- Processing of the data with the proposed automatic method.
- Inspection of the result by an expert neurologist who validates the registration between two successive slices.
- If necessary adjustment of the registration by manually aligning the eventually misregistered slices.

This semi-manually registered volume was then transformed with known rigid transformation parameters. Each slice was transformed using the same procedure as described for the human brain image (random translations varying from -10 to $+10$ pixels and rotations varying from -10 to $+10$ degrees). Table 2 summarizes the registration errors measured in this case (parameter R was set to $R = 3$). As it can be seen, median and mean translation and rotation errors are significantly less than 1 pixel and 1 degree, respectively. Maximum errors are also less than 1 pixel and 1 degree respectively, showing the robustness of the technique.

The method was tested on several real rat brain volumes, exhibiting standard degradations, such as cuts, tears, orientation differences and discontinuities.

Fig. 3 shows an example where standard similarity measures based on the quadratic error function (7) failed (Fig. 3c) to correctly register two consecutive slices (Fig. 3a and b) exhibiting severe distortion, but where the robust registration achieved accurate matching by discarding outliers (Fig. 3d). Cross-correlation give results very close to the one obtained by the quadratic error function.

Fig. 4 presents an example of two sets of consecutive slices exhibiting moderate (Fig. 4a) and severe distortions (Fig. 4b). The image differences before and after registration illustrate the efficiency of the robust registration method and its ability to cope with large image differences.

The difference in accuracy is readily visible on the registration errors shown in Fig. 3(c) and (d), corresponding to the residual image difference after registration.

Table 2

A set of 400 slices of a 3D rat brain autoradiography volume was artificially transformed using different rigid transformation parameters

Registration error statistics			
	Δt_x	Δt_y	$\Delta \theta$
Median	0.14	0.11	0.27
Maximum	0.65	0.63	0.62
Mean \pm S.D.	0.27 \pm 0.14	0.19 \pm 0.11	0.25 \pm 0.15

Each slice was randomly transformed using translations varying from -10 to $+10$ pixels and rotations varying from -10 to $+10$ degrees. Different statistics on the errors for the rigid transformation parameters are presented. Translation errors are expressed in pixels and rotation errors in degrees.

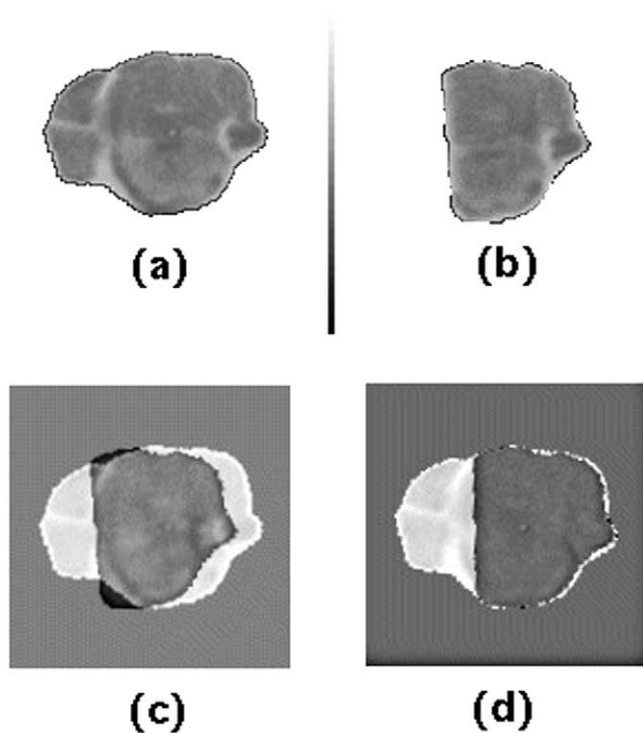


Fig. 3. One set of consecutive slices (a) and (b); (c) difference between the slice (a) and slice (b) after registration using the standard quadratic error function (or cross-correlation); (d) difference between the same slices when the Geman-McClure robust estimation function is used.

Fig. 5 finally present a representative example of real rat brain autoradiographic data reconstruction. As can be seen, the original data is significantly corrupted by distortions, cuts and tears. Slight orientation differences (non-parallel slices) are also observed as well as missing data and discontinuities in the 3D anatomical structures. The slices before registration are shown in Fig. 5(a)–(b) and the result of the registration using the global energy function with the robust pixel similarity measure is presented in Fig. 5(c)–(d). The cuts, tears, missing data and misalignments are clearly visible on the original data, on the multiplanar visualization. The final registrations have been assessed by an expert physician, who has observed a satisfactory alignment of internal as well as external anatomical structures. Let us notice that the algorithm has a computational complexity of $O(n_x n_y N)$ and requires approximately 2 h to register a $128 \times 128 \times 400$ volume on a HP 9000/C200 (200 MHz) workstation.

At last we have registered the 3D reconstructed autoradiographic image on the 3D MRI image of the same rat obtained with a SMIS (UK) 4.7T MRI system. A 40-mm field of view, 256×256 pixel matrix were used as imaging parameters. The whole brain was scanned with a T2-weighted spin-echo fast imaging method sequence (TR:5600/TE:80) by using consecutive 1-mm-thick coronal slices (30 slices). Fig. 6 presents the 3D

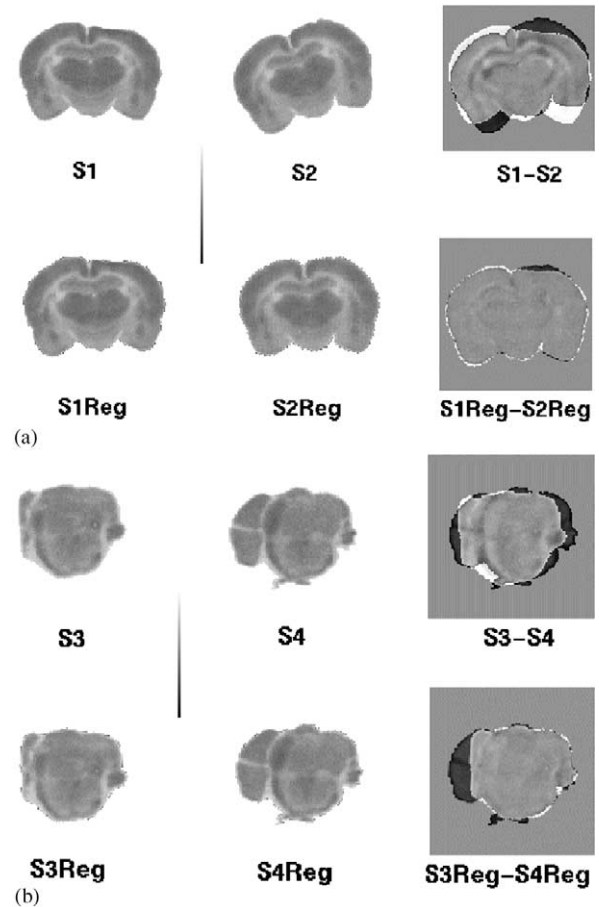


Fig. 4. Two sets of consecutive slices (S1, S2) and (S3, S4) of a rat brain autoradiography. (S1, S2) exhibit moderate distortions (small differences between slices), (S3, S4) show severe distortions (large differences between slices). S1reg, S2reg, S3reg, S4reg are the slices after registration using the robust registration method. The differences between slice S1 and S2 or S3 and S4 are presented before registration (S1–S2) and (S3–S4) and after registration (S1reg–S2reg) and (S3reg–S4reg).

MRI registered on the autoradiographic image by using a fully-automated data-driven registration algorithm. The algorithm, developed by the authors (Nikou et al., 1999), also relies on robust voxel similarity-based metrics, that enable an accurate rigid registration of dissimilar multimodal 3D images. The autoradiographic image is presented in Fig. 6(a) and the 3D MRI, registered with the robust pixel similarity measure, appears in Fig. 6(b). The hippocampus obtained by segmentation of the autoradiography is visualized and superimposed on the two 3D images. The 3D visualization of the hippocampus on Fig. 6 enables to assess the quality of the registration of the autoradiographic slices. The coupling of MRI with autoradiography (through the registration of two 3D images) allows to correlate the morphological changes observed in MRI with the functional modifications observed in autoradiography.

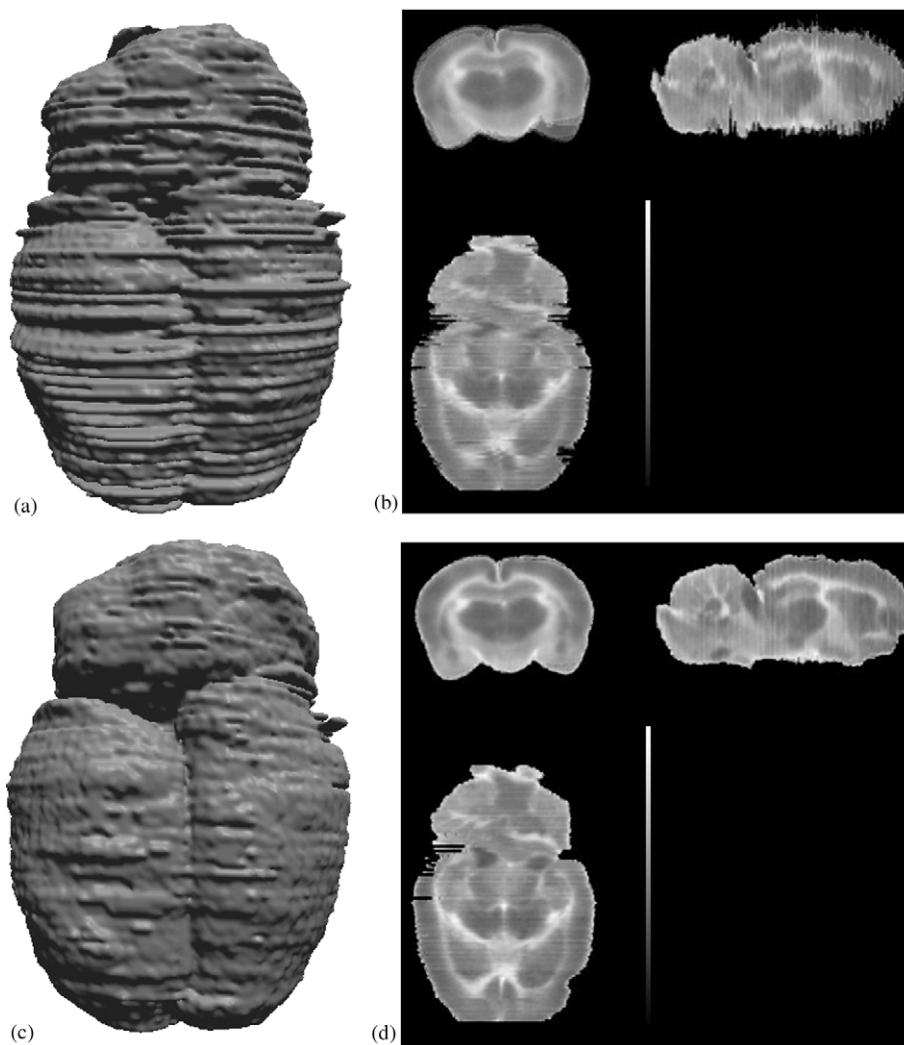


Fig. 5. Reconstruction of a rat brain autoradiography of 400 slices. (a) Three-dimensional view of the volume before registration. (b) Multiplanar view of the volume before registration. (c) Three-dimensional view of the volume after registration. (d) Multiplanar view of the volume after registration.

This method highlights the neuronal networks involved in the pathological process.

5. Conclusion

The alignment method described in this paper has been inspired by the robust voxel similarity metrics-based registration method presented by the authors in [Nikou et al. \(1998\)](#), accounting for inter-image dissimilarities in the case of MRI/SPECT brain image registration. The main contribution of the approach is to consider the alignment of serially acquired sections through the minimization of a global energy function expressing the similarity between two arbitrary sections

in the 3D volume. The approach does not privilege any particular direction in the registration process. By these means, the major problems set by the registration of serially acquired slices are addressed. Thanks to the global (isotropic) formulation of the registration problem (rather than a standard step by step, sequential formulation), no global offset nor error propagations are observed in the final alignment. Besides, gross image differences due to tears, cuts, missing slices or discontinuous anatomical structures are efficiently handled by integrating robust estimation in the similarity measure. The robust function determines whether a measure is an outlier or not, and excludes it from the estimation, providing reliable alignments, even on highly corrupted data.

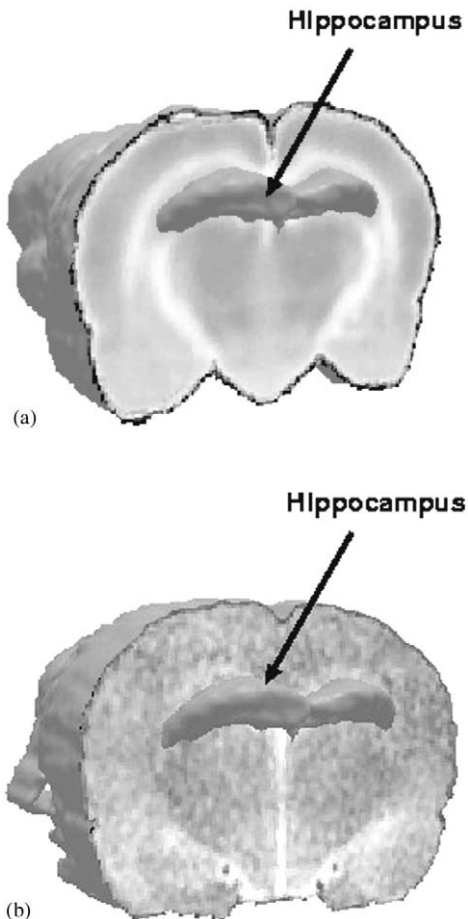


Fig. 6. Registration of a reconstructed autoradiographic image and a 3D MRI. (a) Autoradiographic image. (b) 3D MRI, after multimodal robust registration (see text). The hippocampus obtained after semi-automatic threshold-based segmentation of the autoradiography is visualized and superimposed on the two 3D images.

The proposed robust 3D reconstruction technique will allow the study of volumes of a whole brain structure instead of partial structures obtained from 2D slices. Moreover, by using the standard calibration curve, a 3D image of functional activity may be calculated and superimposed on the morphological 3D brain, obtained by MRI. This operation is usually performed in human brain studies by estimating the blood flow or glucose utilization with SPECT/PET and MR images fusion.

Acknowledgements

We thank Pierre Guntzer for the implementation of the local optimization algorithm discussed in Section 2 and Bertrand Marat for the software implementation in Medimax. This work has been supported by the 'Région Alsace' through the Plan Etat-Region 2000–2006 (Pôle Image).

References

- Alexander M, Somorjai RL. The registration of MR images using multi-scale robust methods. *Magn Reson Imaging* 1996;14(5):453–68.
- Andreasen A, Drewes AM, Assentoft JE, Larsen NE. Computer-assisted alignment of standard serial sections without use of artificial landmarks. A practical approach to the utilization of incomplete information of 3D reconstruction of the hippocampal region. *J Neurosci Methods* 1992;45:199–207.
- Arun KS, Huang TS, Blostein SD. Least squares fitting of two 3D point sets. *IEEE Trans Pattern Anal Mach Intell* 1987;9(3):698–700.
- Black MJ, Jepson AD. Eigen tracking: robust matching and tracking of articulated objects using a view-based representation. In: *Proceedings of the European Conference on Computer Vision*. Cambridge, UK, 1996:1–14.
- Black MJ, Rangarajan A. On the unification of line processes, outliers rejection and robust statistics in early vision. *Int J Comput Vis* 1996;19(1):57–91.
- Goldszal AF, Tretiak OJ, Hand PJ, Bhasin S, Eachron DLM. Three-dimensional reconstruction of activated columns from 2-[¹⁴C] Deoxy-D-glucose data. *NeuroImage* 1995;2(1):9–20.
- Gottesfeld-Brown L. A survey of image registration techniques. *ACM Comput Surv* 1992;24(4):325–76.
- Heitz F, Perez P, Bouthemy P. Multiscale minimization of global energy functions in some visual recovery problems. *Comput Vis Graph Image Proc Image Underst* 1994;59(1):125–34.
- Hess A, Lohmann K, Gundelfinger E, Scheich H. A new method for reliable and efficient reconstruction of 3-dimensional images from autoradiographs of brain sections. *J Neurosci Methods* 1998;84:77–86.
- Hibbard L, Hawkins R. Objective image alignment for three-dimensional reconstruction of digital autoradiographs. *J Neurosci Methods* 1988;26:55–75.
- Huber J. *Robust statistics*. New York: Wiley, 1981.
- Kim B, Boes J, Frey K, Meyer C. Mutual information for automated unwarping of rat brain autoradiographs. *NeuroImage* 1997;5:31–40.
- Maintz JBA, Viergever MA. A survey of medical image registration techniques. *Med Image Anal* 1998;2(1):1–36.
- Meer P, Mintz D, Rosenfeld A, Kim DY. Robust regression methods for computer vision: a review. *Int J Comput Vis* 1990;6(1):59–70.
- Nikou C, Armspach JP, Heitz F, Namer I, Grucker D. MR/MR and MR/SPECT registration of brain images by fast stochastic optimization of robust voxel similarity measures. *NeuroImage* 1998;8(1):30–43.
- Nikou C, Heitz F, Armspach JP. Robust voxel similarity metrics for the registration of dissimilar single and multimodal images. *Pattern Recognit* 1999;32(8):1351–68.
- Odobez JM, Bouthemy P. Robust multiresolution estimation of parametric motion models. *J Vis Commun Image Represent* 1995;6(4):348–65.
- Ourselin S, Roche A, Subsol G, Pennec X, Satttonnet C. Automatic alignment of histological sections for 3D reconstruction and analysis. *Tech. Rep. 3595*, INRIA, Sophia Antipolis, France, 1998.
- Press W, Teukolsky S, Vetterling W, Flannery B. *Numerical Recipes in C—The Art of Scientific Computing*. Cambridge: Cambridge University Press, 1992.
- Rangarajan A, Chui H, Mjolsness E, Pappu S, Davachi L, Goldman-Rakic P, Duncan J. A robust point-matching algorithm for autoradiograph alignment. *Med Image Anal* 1997;1(4):379–98.
- Rousseeuw PJ. Least median of squares regression. *J Am Stat Assoc* 1984;79:871–80.
- Stewart C. Bias in robust estimation caused by discontinuities and multiple structures. *IEEE Trans Pattern Anal Mach Intell* 1997;19(8):818–33.

- Thevenaz P, Blu T, Unser M. Interpolation revisited. *IEEE Trans Med Imaging* 2000;19(7):739–58.
- Toga A, Arnicar T. Image analysis of brain physiology. *Comp Graph Appl* 1985;5(12):20–5.
- Umeyama S. Least-squares estimation of transformation parameters between two point patterns. *IEEE Trans Pattern Anal Mach Intell* 1991;13(4):376–80.
- Van den Elsen P, Paul EJD, Viergever MA. Medical image matching—a review with classification. *IEEE Eng Med Biol* 1993;12(1):26–39.
- Walters F, Parker L, Morgan S, Deming S. *Sequential Simplex Optimization*. Boca Raton, FL: CRC Press, 1991.
- Zhao W, Young T, Ginsberg M. Registration and three-dimensional reconstruction of autoradiographic images by the disparity analysis method. *IEEE Trans Med Imaging* 1993;12(4):782–91.